


Subband-enhanced carrier multiplication in graphene nanoribbonsJunhyeok Bang ^{1,2,*} and Joongoo Kang³¹*Department of Physics, Chungbuk National University, Cheongju 28644, Republic of Korea*²*Research Institute for Nanoscale Science and Technology, Cheongju 28644, Republic of Korea*³*Department of Emerging Materials Science, DGIST, Daegu 42988, Republic of Korea*

(Received 4 November 2020; revised 3 June 2021; accepted 21 June 2021; published 12 July 2021)

Carrier multiplication (CM), which generates multiexcitons from a single photon absorption, is advantageous for increasing the optoelectronic device efficiency. However, CM is intrinsically inefficient in conventional semiconductors, and enhancing CM has been a long-standing challenge. Here, we propose that multisubbands in nanostructures can significantly enhance CM by opening up the intersubband CM transitions, which circumvent the strict restrictions enforced by the energy and momentum conservations. Using real-time time-dependent density functional theory, we demonstrate the mechanism in graphene nanoribbons as an example of a multisubband system. The CM mechanism provides a pathway for developing efficient optoelectronic devices.

DOI: [10.1103/PhysRevB.104.035417](https://doi.org/10.1103/PhysRevB.104.035417)**I. INTRODUCTION**

External perturbations, such as light irradiation and applied voltage, can excite electrons in materials and it leads to a series of dynamic processes, such as carrier thermalization, charge transfer, and recombination [1,2]. The fundamental processes of the excited carriers are crucial for understanding the microscopic working principles of electronic and optoelectronic devices. During the initial stage of the excitation, the excited carrier undergoes thermalization by carrier-carrier scattering, wherein the excess energy of the excited carrier is transferred to a background electron, and carrier-lattice scattering, whereby the carrier energy is converted to thermal vibration of the lattice [1–4]. Under certain conditions (discussed below), the carrier-carrier scattering can excite another valence electron to the conduction band across the band gap of a semiconductor, as illustrated in Fig. 1(a). This phenomenon is called carrier multiplication (CM). The absorption of a single photon can generate more than one electron-hole pair via CM. Therefore, this phenomenon enables an increase in the power conversion efficiencies over the Shockley-Queisser limit in photovoltaics [5,6]. Moreover, it can also enhance the responsivity of photodetectors and scintillators [7,8].

In CM, both energy and momentum of the excited electron (electron 1) are transferred to the valence electron (electron 2), as shown in Fig. 1(a). The total energy and momentum should be simultaneously conserved in a scattering process. Thus, CM is only possible when electron 2 is initially in a specific valence state so that it is excited onto a state in the conduction band by the transferred energy and momentum. This condition considerably restricts the CM process in conventional semiconductors [9–11]. For instance, if we consider single parabolic valence and conduction bands having the same effective masses, then CM is possible only when the

excess energy of electron 1 is more than four times higher than the band gap [12]. In addition, the existence of highly efficient competing energy loss channels to lattices further reduces the probability of CM in conventional semiconductors [9].

However, CM can be enhanced in special materials that are designed by considering the two limiting factors: the energy-momentum conservation and the carrier-lattice scattering. Quantum dots (QDs) are an example of such systems. In the QDs, the energy loss to the lattices is significantly suppressed owing to the large energy spacing between their quantized levels. The first theoretical concept of CM using the phonon bottleneck was suggested in 2002 [13,14] and later experimentally observed in PbSe, PbS, CdSe, InAs, and Si QDs [15–19]. Another example is graphene. Because graphene has a peculiar linear band dispersion around the Dirac point, the energy and momentum conservation can be easily satisfied leading to efficient CM [9–11,20,21]. However, graphene has zero band gap, and thus, the electron-hole recombination occurs quickly, making it difficult to extract and use the generated excited carriers [11]. The carrier lifetime can be increased in graphene nanoflakes [22–24] and graphene nanoribbons (GNRs) [25] via quantum confinement, which opens a band gap in such zero band gap materials. The graphene nanoflakes have quantized energy levels, and thus, CM may occur in them due to phonon bottleneck effects, similar to semiconductor QDs. In contrast, GNRs are a different class of materials having one-dimensional (1D) periodic structures. As a result, they neither possess linear band structures like graphene nor quantized energy levels like QDs. Thus, it is not clear whether CM can occur in GNRs.

The theoretical investigation of the excited state dynamics and CM requires two important considerations that are generally ignored in most static state calculations. First, a dynamic change in the system induced by ultrafast carrier dynamics should be considered. In this case, the carrier scattering rates are no longer constant but change with time [1–4]. Second, the theoretical calculations should include all

*Corresponding author: jbang@cbnu.ac.kr

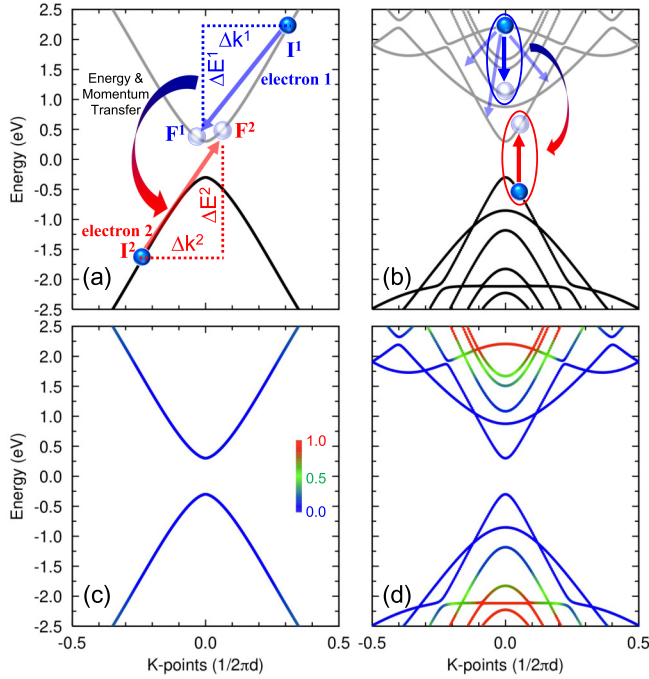


FIG. 1. Schematic diagram of the CM process in (a) single band and (b) multisubband models. In CM, as shown in (a), both energy ΔE^1 and momentum Δk^1 of the excited electron (electron 1) are transferred to the electron in the valence band (electron 2), and electron 2 is excited to the conduction band. In (b), intersubband transitions increase the number of possible CM processes. We represent the calculated $N(I^1)$ using the color coding in (c) the single band and (d) the multisubband models. We normalized $N(I^1)$ by dividing it by the maximum value shown in (d). In (b) and (d), we have used the band structure of 12 AGNR.

competing processes caused by the carrier-carrier and carrier-lattice scatterings [3,4,26]. For instance, although the CM rate is high, the CM process becomes inefficient when the rate of the competing carrier-lattice scattering is even higher than the CM rate. In this study, we investigated the carrier dynamics using real-time time-dependent density functional theory (TDDFT), which considers both the aforementioned factors, and found that CM indeed occurs in GNRs. As shown in Fig. 1(b), the multisubbands, which are a distinct feature of GNRs, play a key role in CM by allowing the intersubband transitions, thereby increasing the number of CM processes satisfying the energy and momentum conservations. Furthermore, we observed strongly correlated electron-ion dynamics in the ultrafast regime, controlled by the electronic structure of GNRs. This provides a way to control the carrier dynamics and CM in GNRs by changing the ribbon width and edge type.

II. CALCULATION METHODS

Real-time electron and ion dynamics has been simulated based on the TDDFT-molecular dynamics (MD) calculation [27], which was implemented in the code developed based on the SIESTA program [28–30]. The Troullier-Martins norm-conserving pseudopotentials [31] and local density-functional approximation for the exchange-correlation potential [32]

were employed in our calculations. Wave functions were expanded using a localized basis set with double- ζ polarized orbitals. The real-space grid used in the calculations is equivalent to a plane-wave cutoff energy of 200 Ry. We used periodic supercells of armchair GNRs (AGNRs) containing 156–192 atoms. Γ -point sampling was used in the Brillouin zone integration. In the calculations of the dynamics, we used a time step of 12.5 attoseconds and applied the Ehrenfest approximation for ion dynamics, which uses the Newton's equation in which the electronic energy is considered as the ionic potential. These TDDFT-MD calculations can describe the electron-ion energy exchange, i.e., the transfer of energy from the excited electron to the ionic kinetic energy by carrier-lattice scattering. Further, a microcanonical (or NVE) ensemble was used to measure the effect of the carrier-lattice scattering. To prepare the input structures of the TDDFT-MD simulations, we performed electronic ground-state MD simulations and extracted the equilibrated atomic coordinates and velocities at room temperature (300 K). The temperature dependence of CM is also an important factor to be considered in electronic excited state dynamics, although its effects on the dynamics is under debate [33,34]. In this work, however, we focused only on the subband effect, and thus, fixed the initial ionic temperature to 300 K for all the simulations. To mimic optical excitation, the electron in the valence band was excited to the conduction band by changing the band occupations [35,36]. For obtaining statistically unbiased results, we considered ensembles in the TDDFT-MD simulations, wherein each one was simulated five times with different initial atomic coordinates and velocities. All the simulated ensembles yielded the same qualitative results.

As a wave function evolves in time according to the time-dependent Kohn-Sham equation [27], it cannot be cast as an energy eigenstate of the system Hamiltonian. Instead, we can represent the time-evolved Kohn-Sham wave function $|\psi_i(t)\rangle$ of the i th state using the basis states $|\phi_j(t)\rangle$ at time t using the following equation:

$$|\psi_i(t)\rangle = \sum_j |\phi_j(t)\rangle \langle \phi_j(t) | \psi_i(t) \rangle = \sum_j a_{ij}(t) |\phi_j(t)\rangle,$$

where $a_{ij}(t) = \langle \phi_j(t) | \psi_i(t) \rangle$. Here, we used the adiabatic energy eigenstates $|\phi_j(t)\rangle$ of the system Hamiltonian $\hat{H}[\{R(t)\}, \rho(t)]$ as the basis states. Because $\hat{H}[\{R(t)\}, \rho(t)]$ is a functional of the atomic configuration $\{R(t)\}$ and electron density $\rho(t)$, both of which are time-dependent quantities, the adiabatic energy eigenstates also change with time. Because $|a_{ij}(t)|^2$ is the probability that a carrier in the i th time-evolved state is found in the j th adiabatic state, the time-evolved electron occupation $n_j(t)$ in the j th adiabatic state can be calculated by [37–39]

$$n_j(t) = \sum_i |a_{ij}(t)|^2.$$

We analyzed the excited carrier dynamics using this time-dependent electron occupations.

III. RESULTS AND DISCUSSION

We consider electron 1, which undergoes a transition from the initial state I^1 to the final state F^1 , as shown in Fig. 1(a).

Here, the initial wave vector k_i^1 and energy E_i^1 change into the final wave vector k_f^1 and energy E_f^1 . We denote the changes in the wave vector and energy of electron 1 as $\Delta k^1 = k_f^1 - k_i^1$ and $\Delta E^1 = E_f^1 - E_i^1$, respectively. To satisfy the energy and momentum conservations, the changes in the wave vector, $\Delta k^2 (= k_f^2 - k_i^2)$, and energy, $\Delta E^2 (= E_f^2 - E_i^2)$, of electron 2 [see Fig. 1(a)] should fulfill the conditions $\Delta E^1 + \Delta E^2 = 0$ and $\Delta k^1 + \Delta k^2 = 0$. For the given transition of electron 1, the number of allowed CM processes, $t(I^1, F^1)$, is expressed as

$$t(I^1, F^1) = \sum_{v_i^1, v_f^1} \int dk_i^1 dk_f^1 \delta(\Delta E^1 + \Delta E^2) \delta(\Delta k^1 + \Delta k^2).$$

Here, v_i^1 and v_f^1 are the initial valence band and final conduction band indices, respectively, of electron 1. This is similar to the joint density of state; however, a change in the wave vector is included here. Although we assume that the excited particle is an electron in the conduction band, the same formula can be applied to an excited hole as well. By integrating out the final state F^1 , the number of the allowed CM processes for the initial state I^1 is given by

$$N(I^1) = \sum_{v_i^1} \int dk_f^1 t(I^1, F^1).$$

If the matrix elements are nearly same for all the CM transitions, then the CM rate is proportional to $N(I^1)$. Because $N(I^1)$ is determined solely by the band structure of a system, one can increase or decrease the CM rate by modifying the band structure.

Figure 1(c) shows the calculated $N(I^1)$ for the single band model [Fig. 1(a)]. In the given energy region $|E_i^1| < 2.5$ eV, $N(I^1)$ is zero or negligible. In the single band, the changes in the wave vectors and energies of electron 1 and electron 2 (Δk^1 , Δk^2 , ΔE^1 and ΔE^2) are very limited. Therefore, the transition satisfying both the conditions— $\Delta k^1 = -\Delta k^2$ and $\Delta E^1 = -\Delta E^2$ —is rare in the given band structure. To enhance $N(I^1)$, one can increase the phase space of both (Δk^1 , ΔE^1) and (Δk^2 , ΔE^2) by introducing subbands into the band structure, which allow the intersubband transitions as shown in Fig. 1(b). Figure 1(d) shows the calculated $N(I^1)$ for such a multisubband model. Although $N(I^1)$ is still small in the lower conduction bands and upper valence bands, it is significantly enhanced in the *core* subbands. This is because the intersubband transitions, as shown in Fig. 1(b), increase the number of CM processes satisfying the energy and momentum conservations. $N(I^1)$ for the multisubband model exhibits more than a 20-fold increase as compared to that for the single-band model shown in Fig. 1(c).

AGNRs are good examples of multisubband systems. In fact, Figs. 1(b) and 1(d) are the band structure of AGNR with 12 dimer lines. Following the previous convention [25,40], we refer to an AGNR with N dimer lines across the ribbon width [see Fig. 2(a)] as N AGNR. The band structure of an AGNR depends on the number of the dimer lines. As the size of a nanomaterial decreases, its band gap tends to increase owing to the quantum confinement effect. Additionally, the AGNR band structure can undergo band-gap modulation with a periodicity of three dimer lines [25,41]; that is, in the N

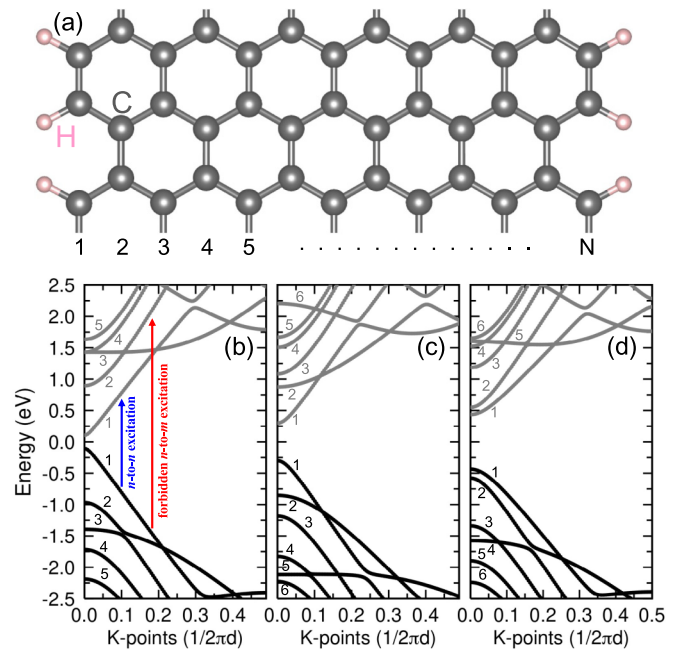


FIG. 2. Ball and stick model of (a) the atomic structure of N AGNR, and the band structures of (b) 11 AGNR, (c) 12 AGNR, and (d) 13 AGNR. The numbers in (a) and (b)–(d) represent the dimer lines and subband indices, respectively. Blue and red arrows in (b) indicate the allowed n -to- n excitation and forbidden n -to- m excitation, respectively, by the polarized light along the longitudinal direction of AGNRs.

AGNR, the smallest band gap occurs for $N = 3m - 1$, and the largest band gap occurs for $N = 3m + 1$ for the same positive integer number m . Here, we consider 11, 12, and 13 AGNRs with band gaps of 0.21, 0.60, and 0.87 eV, respectively [see Figs. 2(b)–2(d)]. Recently, tremendous progress has been made in developing advanced fabrication techniques to engineer high-quality GNRs, and the existence of the band-gap modulation effect has been verified in atomically well-controlled AGNRs [42,43].

Figures 3(a)–3(c) show the complex dielectric functions (ϵ_2) of the AGNRs. The AGNRs exhibit strong polarization anisotropy in the optical absorption spectrum, which originates from the polarization-dependent optical selection rule [44,45]. In the polarization along the longitudinal direction of an AGNR, the optical selection rule allows only direct transition from the valence band to the conduction band with the same subband indices: As represented in Fig. 2(b), an excitation from the n th valence band to the n th conduction band (n -to- n excitation) is allowed; however, an n -to- m excitation ($n \neq m$) is not allowed. Owing to the large joint density of states around the subband edges at the Γ point, the complex dielectric functions also show sharp peaks for the corresponding n -to- n excitations at the Γ point. Thus, by tuning the polarized light frequency to a peak resonance, one can selectively populate holes at the n th valence-band edge and electrons at the n th conduction-band edge, thereby placing the excited carriers on the *core* subband edge. Notably, the selective n -to- n excitation leaves other energy levels unoccupied. This is also advantageous for the CM process because

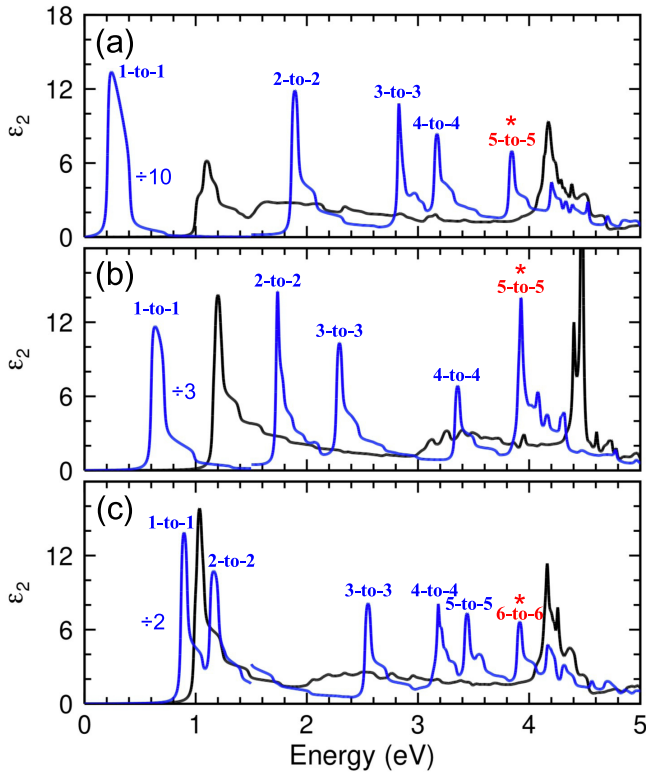


FIG. 3. Complex dielectric function (ϵ_2) of (a) 11 AGNR, (b) 12 AGNR, and (c) 13 AGNR excited by polarized light along the direction parallel to the ribbon width (black) and longitudinal direction of AGNR (blue). The corresponding n -to- n excitation peaks are designated by blue lines, and the data below 1.5 eV have been rescaled by dividing them by factors of 10, 3, and 2 in (a)–(c), respectively.

the carrier occupations on the lower energy levels reduce CM via Pauli blocking [10,11].

We considered such an optical n -to- n excitation and simulated the excited carrier dynamics using TDDFT-MD calculations. For a reasonable comparison between the three AGNRs, we focus on the n -to- n excitation around 3.9 eV (see Fig. 3), which corresponds to the 5-to-5 excitation for 11 and 12 AGNRs and the 6-to-6 excitation for 13 AGNR. Figure 4(a) shows the excited carrier dynamics in 12 AGNR, represented by the electron occupations on each energy level at given times. The electron occupations are calculated by projecting the time-evolved TDDFT wave functions onto the adiabatic states at a given time, as described in the calculation method section. The time evolutions of the electron occupations in the 11 and 13 AGNRs are qualitatively similar to that in the 12 AGNR. The excited electron and hole [denoted by pink and blue, respectively, in Fig. 4(a)] undergo ultrafast relaxation during the first several hundred femtoseconds. This is the thermalization process, which takes place in the initial stage of the excitation, as discussed in Refs. [1,2]. During the process, the electron occupation approaches the Fermi-Dirac distribution at 3000 K due to the carrier-carrier and carrier-lattice scatterings. Notably, 3000 K is the only electronic temperature; the ionic temperature is far below this value [see Fig. 4(c)]. The nonequilibrium condition usually occurs in the excited state

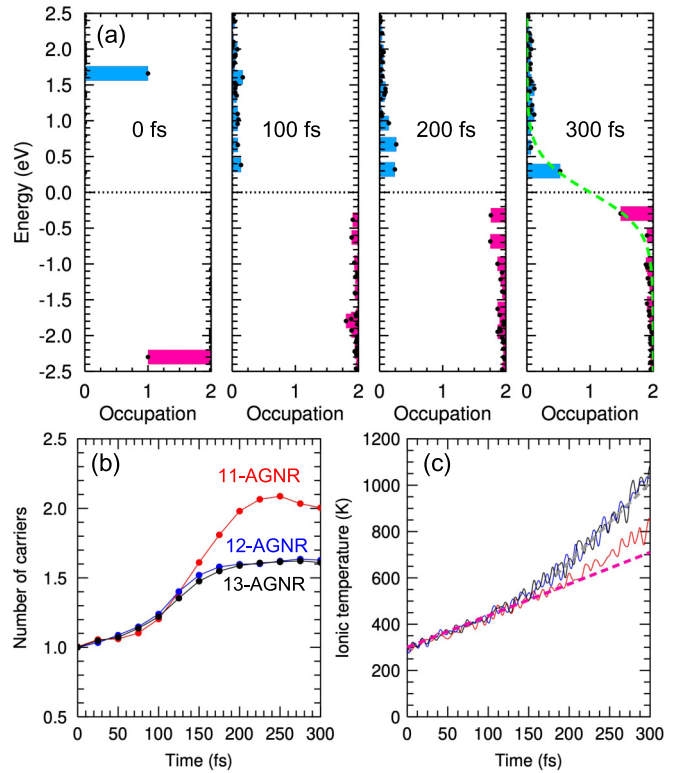


FIG. 4. Time evolution of (a) electron (pink) and hole (blue) occupation on each energy level, (b) the number of excited carriers, and (c) the ionic temperature. The green dashed curve in the 300 fs panel in (a) is the Fermi-Dirac distribution at 3000 K. In (b) and (c), red, blue, and black curves represent the results of 11, 12, and 13 AGNRs, respectively. In (c), the slopes of the pink and gray dashed curves are 1.67 and 3.2 K/fs, respectively.

dynamics. The electronic system is still in the thermalization process at 300 fs; therefore, the electron occupation is slightly deviated from the Fermi-Dirac distribution. We counted the total number of excited electrons in the conduction bands and plotted its time variation in Fig. 4(b). Notably, the total number of the excited holes in the valence bands is equal to that of the excited electrons owing to charge neutrality. For all the AGNRs, the number of the excited carriers increases during the thermalization, which clearly indicates that CM occurs in the AGNRs.

Figure 4(b) shows the different behaviors of CM in the AGNRs. In 12 and 13 AGNRs, the number of carriers increases to 1.6 until 175 fs, and then it remains nearly constant around the maximum value. In 11 AGNR, on the other hand, the number of carriers further increases and finally reaches 2.1 at 250 fs. The results can be understood in terms of the excess energy of the excited carrier, which is measured from the band edges, i.e., conduction band minimum for electrons and valence band maximum for holes. In the CM process, as shown in Fig. 1(a), the excess energy of electron 1 should be larger than the band gap of the system to facilitate the excitation of electron 2 to the conduction band. The 12 and 13 AGNRs have relatively large band gaps (0.60 eV for 12 AGNR and 0.87 eV for 13 AGNR), and thus the initially excited carrier spends considerable energy in generating another carrier. After the first CM process,

the excess energy of the carrier is not sufficient to generate more carriers. In contrast, the 11 AGNR has a relatively small band gap (0.21 eV); thus, it requires a small energy and the initial excited carrier can generate more carriers. Our results shown in Fig. 4(b) clearly reflect the band-gap dependence of CM.

The band gap is a key physical parameter in understanding the competition between the different relaxation channels and in controlling the coupled electron-ion dynamics. Figure 4(c) shows the time variation of the ionic temperature, which is a good measure of the carrier-lattice scattering because we used an *NVE* ensemble. As shown in Fig. 4(c), the ionic temperatures increase owing to the energy transfer from the excited carrier to the lattice by the carrier-lattice scattering. These ionic temperatures increase to approximately 850 K in the 11 AGNR and nearly 1050 K in 12 and 13 AGNRs until 300 fs. In the simulation time scale, the systems maintain their original AGNR structures, with thermal vibration, and are stable. The slopes of the temperature curves for the three AGNRs (1.37 K/fs) are similar in the initial stage. However, they branch at around 150 fs; the slopes increase to 3.2 K/fs in both 12 and 13 AGNRs, while that in 11 AGNR remains unchanged. In the initial stage, both the competing processes, i.e., CM by carrier-carrier scattering and energy transfer by carrier-lattice scattering, are possible in all the AGNRs, and the excited carrier energy is distributed to both degrees of freedom. In 12 and 13 AGNRs, however, the CM relaxation channel slows down at 150 fs, as discussed earlier, and subsequently only the carrier-lattice scattering remains as the sole relaxation channel. Thus, more energy can be transferred to the lattice, thereby increasing the slope. In 11 AGNR, on the other hand, the CM process persists, and the amount of the transferred energy does not change until 200 fs. Later, the slope also increases for the same reason. The anticorrelation between the CM process and energy transfer, which is ruled

by the band gap, provides a way to control the excited state dynamics in the ultrafast regime.

The band gap also affects the carrier recombination. The small band gap in 11 AGNR is very close to the optical phonon energy [46], due to which electron-hole recombination can occur via carrier-lattice scattering. As a result, the number of excited carriers starts decreasing at 250 fs. However, such recombination cannot occur in 12 and 13 AGNRs because of their large band gaps. Thus, the number of carriers remains unchanged following the CM process.

IV. SUMMARY

In summary, we have shown that CM occurs in AGNRs using real-time TDDFT-MD simulations. The key message here is that subbands can enhance CM as they can circumvent the strong restriction imposed by the energy and momentum conservations. This concept for developing smart and efficient optoelectronic devices may facilitate better understanding of the previously reported CM experiments, such as the highly efficient, yet mysterious, CM observed in transition metal dichalcogenides, whose band structures consist of atomic *d* orbitals [47].

ACKNOWLEDGMENTS

J.B. was supported by Basic Science Research Program through the National Research Foundation of Korea (NRF) (Grants No. NRF-2018R1D1A1B07044564 and No. NRF-2020R1A4A1019566) and the National Research Council of Science & Technology (Grant No. CAP-18-05-KAERI). J.K. was supported by an NRF grant funded by the Korean government (MSIP) (Grant No. 2016R1C1B2016046). We used the VESTA software to generate Fig. 2(a) [48].

-
- [1] S. K. Sundaram and E. Mazur, *Nat. Mater.* **1**, 217 (2002).
 - [2] J. Shah, *Ultrafast Spectroscopy of Semiconductors and Semiconductor Nanostructures* (Springer, Berlin, 1991).
 - [3] J. Bang, S. Meng, Y.-Y. Sun, D. West, Z. Wang, F. Gao, and S. B. Zhang, *Proc. Natl. Acad. Sci. USA* **110**, 908 (2013).
 - [4] J. Bang, Y. Y. Sun, X.-Q. Liu, F. Gao, and S. B. Zhang, *Phys. Rev. Lett.* **117**, 126402 (2016).
 - [5] W. Shockley and H. J. Queisser, *J. Appl. Phys.* **32**, 510 (1961).
 - [6] V. Shukhovatkin, S. Hinds, L. Brzozowski, and E. H. Sargent, *Science* **324**, 1542 (2009).
 - [7] M. Nikl, *Phys. Status Solidi A* **178**, 595 (2000).
 - [8] J. Bang, Z. Wang, F. Gao, S. Meng, and S. B. Zhang, *Phys. Rev. B* **87**, 205206 (2013).
 - [9] N. M. Gabor, *Acc. Chem. Res.* **46**, 1348 (2013).
 - [10] T. Winzer, A. Knorr, and E. Malic, *Nano Lett.* **10**, 4839 (2010).
 - [11] E. Malic, T. Winzer, F. Wendler, and A. Knorr, *Phys. Status Solidi B* **253**, 2303 (2016).
 - [12] Y. Kanemitsu, *Acc. Chem. Res.* **46**, 1358 (2013).
 - [13] A. J. Nozik, *Phys. E (Amsterdam, Neth.)* **14**, 115 (2002).
 - [14] A. J. Nozik, *Chem. Phys. Lett.* **457**, 3 (2008).
 - [15] R. D. Schaller and V. I. Klimov, *Phys. Rev. Lett.* **92**, 186601 (2004).
 - [16] R. J. Ellingson, M. C. Beard, J. C. Johnson, P. Yu, O. I. Micic, A. J. Nozik, A. Shabaev, and A. L. Efros, *Nano Lett.* **5**, 865 (2005).
 - [17] R. D. Schaller, M. Sykora, S. Jeong, and V. I. Klimov, *J. Phys. Chem. B* **110**, 25332 (2006).
 - [18] R. D. Schaller, J. M. Pietryga, and V. I. Klimov, *Nano Lett.* **7**, 3469 (2007).
 - [19] M. C. Beard, K. P. Knutsen, P. Yu, J. M. Luther, Q. Song, W. K. Metzger, R. J. Ellingson, and A. J. Nozik, *Nano Lett.* **7**, 2506 (2007).
 - [20] K. J. Tielrooij, J. C. W. Song, S. A. Jensen, A. Centeno, A. Pesquera, A. Z. Elorza, M. Bonn, L. S. Levitov, and F. H. L. Koppens, *Nat. Phys.* **9**, 248 (2013).
 - [21] D. Brida, A. Tomadin, C. Manzoni, Y. J. Kim, A. Lombardo, S. Milana, R. R. Nair, K. S. Novoselov, A. C. Ferrari, G. Cerullo, and M. Polini, *Nat. Commun.* **4**, 1987 (2013).
 - [22] L. Ci, L. Song, C. Jin, D. Jariwala, D. Wu, Y. Li, A. Srivastava, Z. F. Wang, K. Storr, L. Balicas, F. Liu, and P. M. Ajayan, *Nat. Mater.* **9**, 430 (2010).

- [23] D. Chen, R. Qiao, X. Xu, W. Dong, L. Wang, R. Ma, C. Liu, Z. Zhang, M. Wu, L. Liu, L. Bao, H.-T. Wang, P. Gao, K. Liu, and D. Yu, *Nanoscale* **11**, 4226 (2019).
- [24] Y. Zhou, Z. Wang, P. Yang, and F. Gao, *J. Phys. Chem. C* **116**, 7581 (2012).
- [25] Y.-W. Son, M. L. Cohen, and S. G. Louie, *Phys. Rev. Lett.* **97**, 216803 (2006).
- [26] H. Wang, J. Bang, Y. Sun, L. Liang, D. West, V. Meunier, and S. B. Zhang, *Nat. Commun.* **7**, 11504 (2016).
- [27] E. Runge and E. K. U. Gross, *Phys. Rev. Lett.* **52**, 997 (1984).
- [28] J. M. Soler, E. Artacho, J. D. Gale, A. Garcia, J. Junquera, P. Ordejon, and D. Sanchez-Portal, *J. Phys.: Condens. Matter* **14**, 2745 (2002).
- [29] S. Meng and E. Kaxiras, *J. Chem. Phys.* **129**, 054110 (2008).
- [30] O. Sugino and Y. Miyamoto, *Phys. Rev. B* **59**, 2579 (1999).
- [31] N. Troullier and J. L. Martins, *Phys. Rev. B* **43**, 1993 (1991).
- [32] D. M. Ceperley and B. J. Alder, *Phys. Rev. Lett.* **45**, 566 (1980).
- [33] H.-D. Kim and O. V. Prezhdo, *Nano Lett.* **11**, 1845 (2011).
- [34] S. Cate, Y. Liu, J. M. Schins, M. Law, and L. D. A. Siebbeles, *J. Phys. Chem. Lett.* **4**, 3257 (2013).
- [35] S. M. Falke, C. A. Rozzi, D. Brida, M. Maiuri, M. Amato, E. Sommer, A. D. Sio, A. Rubio, G. Cerullo, E. Molinari, and C. Lienau, *Science* **344**, 1001 (2014).
- [36] S. Meng and E. Kaxiras, *Nano Lett.* **10**, 1238 (2010).
- [37] D. Han, J. Bang, W. Xie, V. Meunier, and S. B. Zhang, *J. Phys. Chem. Lett.* **7**, 3548 (2016).
- [38] M. A. Zeb, J. Kohanoff, D. Sanchez-Portal, A. Arnau, J. I. Juaristi, and E. Artacho, *Phys. Rev. Lett.* **108**, 225504 (2012).
- [39] J. Bang, S. Meng, and S. B. Zhang, *Phys. Rev. B* **100**, 245208 (2019).
- [40] D. H. Choe, J. Bang, and K. J. Chang, *New J. Phys.* **12**, 125005 (2010).
- [41] L. Yang, C.-H. Park, Y.-W. Son, M. L. Cohen, and S. G. Louie, *Phys. Rev. Lett.* **99**, 186801 (2007).
- [42] W.-X. Wang, M. Zhou, X. Li, S.-Y. Li, X. Wu, W. Duan, and L. He, *Phys. Rev. B* **93**, 241403(R) (2016).
- [43] W. Xu and T.-W. Lee, *Mater. Horiz.* **3**, 186 (2016).
- [44] K. I. Sasaki, K. Kato, Y. Tokura, K. Oguri, and T. Sogawa, *Phys. Rev. B* **84**, 085458 (2011).
- [45] H. Hsu and L. E. Reichl, *Phys. Rev. B* **76**, 045418 (2007).
- [46] R. Gillen, M. Mohr, J. Maultzsch, and C. Thomsen, *Phys. Rev. B* **80**, 155418 (2009).
- [47] J.-H. Kim, M. R. Bergren, J. C. Park, S. Adhikari, M. Lorke, T. Frauenheim, D.-H. Choe, B. Kim, H. Choi, T. Gregorkiewicz, and Y. H. Lee, *Nat. Commun.* **10**, 5488 (2019).
- [48] K. Momma and F. Izumi, *J. Appl. Crystallogr.* **44**, 1272 (2011).